ASCE

Seismic Response of Post-Tensioned Cross-Laminated Timber Rocking Wall Buildings

Alex W. Wilson[1]; Christopher J. Motter[2]; Adam R. Phillips[3]; and J. Daniel Dolan[4]

Abstract: Nonlinear time history analyses were conducted for 5-story and 12-story prototype buildings that used post-tensioned cross-laminated timber rocking walls coupled with U-shaped flexural plates (UFPs) as the lateral force resisting system. The building models were subjected to 22 far-field and 28 near-fault ground motions, with and without directivity effects, scaled to the design earthquake and maximum considered earthquake for Seattle, with Site Class D. The buildings were designed to performance objectives that limited structural damage to crushing at the wall toes and nonlinear deformation in the UFPs, while ensuring code-based interstory drift requirements were satisfied and the post-tensioned rods remained linear. The walls of the 12-story building had a second rocking joint at midheight to reduce flexural demands in the lower stories and interstory drift in the upper stories. The interstory drift, in-plane wall shear and overturning moment, UFP deformation, and extent of wall toe crushing is summarized for each building. Near-fault ground motions with directivity effects resulted in the largest demands for the 5-story building, while the midheight rocking joint diminished the influence of ground motion directivity effects in the 12-story building. Results for both buildings confirmed that UFPs located higher from the base of the walls dissipated more energy compared to UFPs closer to the base. **DOI:** 10.1061/(ASCE)ST.1943-541X.0002673.

Author keywords: Cross-laminated timber (CLT); Self-centering; Nonlinear response history analysis; Near-field earthquakes; Structural wall.

Introduction

Structural walls are often used in buildings to resist lateral force demands from earthquake and wind loads. While the use of concrete and steel structural systems is commonplace, the use of cross-laminated timber (CLT) walls may be a viable alternative. Although gravity load resisting CLT structural components are included in current US building codes and design standards, seismic lateral force resisting CLT systems are not. CLT originated in regions of central Europe where design-level seismic demands are generally less than in the western United States, where the design of lateral force resisting systems is often controlled by seismic loading. The US building codes allow for inelastic component behavior during seismic events, but require this behavior to be ductile and predictably concentrated at specific locations for control of building response. A self-centering post-tensioned (PT) CLT rocking wall lateral system is intended to minimize wall damage during seismic events (Pei et al. 2018). During rocking, inelastic deformation is limited to the wall toes and the hysteretic coupling devices that connect adjacent wall segments, while the PT rods provide a self-centering restoring force to minimize residual drift.

In prescriptive, code-based building design, inelastic behavior is typically accounted for by using elastic analysis and seismic response factors specific to a lateral force resisting system. Seismic response factors in ASCE 7 consist of the response modification coefficient (R), overstrength factor (Ω_o), and deflection amplification (C_d) factors, which are intended to predict the inelastic response of a system from the response of an elastic analysis (ASCE 2017). To determine seismic response factors for new systems and introduce them into the building code, a FEMA P-695 (ATC 2009) study is typically conducted, but this process is resource-intensive due to the extent of the nonlinear time-history analyses required. Therefore, many newly developed structural systems, such as self-centering PT CLT rocking walls, do not have established seismic response factors.

As an alternative to code-based design, many jurisdictions in the US allow performance-based seismic design (PBSD) using nonlinear time history (NLTH) analysis. PBSD involves meeting performance objectives based on acceptance criteria that are intended to meet or exceed building code expectations. Seismic performance objectives typically target behavior at the design earthquake (DE) and maximum considered earthquake (MCE_R) event magnitudes, where inelastic behavior is expected (PEER 2017). Performance objectives and acceptance criteria are explicitly assessed through NLTH analyses, where component behavior is typically modeled using results from experimental testing. The results of NLTH analysis are highly dependent on the dynamic characteristics of a structure, as well as the ground motions utilized for assessment (Chopra 2012). Depending on the site location, the hazard may consist of far-field and/or near-fault earthquakes. These two ground motion types possess different velocity and acceleration trace characteristics, leading to different building responses, which may result in significantly different demands.

To implement PT CLT rocking wall systems in buildings located in high seismic regions using PBSD, an understanding of dynamic

[1]Design Engineer, Magnusson Klemencic Associates, Seattle, WA 98101; formerly, Graduate Research Assistant, Dept. of Civil and Environmental Engineering, Washington State Univ., Pullman, WA 99164. Email: alex.wilson@wsu.edu

[2]Assistant Professor, Dept. of Civil and Environmental Engineering, Washington State Univ., Pullman, WA 99164. Email: c.motter@wsu.edu

[3]Assistant Professor, Dept. of Civil and Environmental Engineering, Washington State Univ., Pullman, WA 99164. ORCID: https://orcid.org/0000-0003-2486-6039. Email: a.phillips@wsu.edu

[4]Professor, Dept. of Civil and Environmental Engineering, Washington State Univ., Pullman, WA 99164 (corresponding author). Email: jddolan@wsu.edu

Note. This manuscript was submitted on August 9, 2019; approved on January 25, 2020No Epub Date. Discussion period open until 0, 0; separate discussions must be submitted for individual papers. This paper is part of the ***Journal of Structural Engineering***, © ASCE, ISSN 0733-9445.

and inelastic response under likely ground motion types is necessary. This paper presents the NLTH analysis and the resulting global and local responses of a 5- and 12-story PT CLT rocking wall prototype building designed to exhibit inelastic response at the wall toes and in the hysteretic damping devices when subjected to DE level events, with further inelastic response at MCE_R level events. To investigate the influence of ground motion type, a total of 50 records from the Pacific Earthquake Engineering Research (PEER) Center NGA-West 2 ground motion database (PEER 2018), representative of both far-field and near-fault events, were utilized for NLTH analysis, with the records scaled to DE and MCE_R intensity levels for a representative high seismic acceleration region.

85 Background

Research on PT rocking walls was initially conducted for precast concrete walls (Priestley et al. 1999; Kurama et al. 1999a, b; Perez et al. 2013). Studies on the use of supplemental energy dissipation in PT precast concrete rocking walls included adjacent walls with energy dissipating connectors along the height (Nakaki et al. 1999), walls connected to adjacent columns by energy dissipaters (Sritharan et al. 2015; Twigden et al. 2017), and mild steel bars connecting the wall to the foundation to provide energy dissipation at the base (Kurama 2002; Holden et al. 2003; Restrepo and Rahman 2007; Smith et al. 2011). Many of these concepts for PT precast concrete rocking walls were extended to PT LVL rocking walls (Sarti et al. 2016a, b, c) and PT CLT rocking walls (Ganey et al. 2017; Akbas et al. 2017).

PT CLT rocking walls, which were considered in this study, consist of vertically oriented CLT panels with unbonded PT rods along their center lines. The force couple between the PT rods and compression at the wall toe provides resistance to the moment created by lateral loads at the base of the wall. The initial PT stress compresses the wall panels, preventing rocking from occurring at the base until the overturning moment at the base exceeds the decompression moment. Once the decompression moment is exceeded, uplift occurs as the wall rocks about its toe. Rocking leads to an increase in rod stress due to elongation and may cause inelastic behavior in compression at the toe. The use of steel U-shaped flexural plates (UFPs) located between adjacent wall panels provides additional strength and stiffness through coupling and provides enhanced energy dissipation through hysteretic damping (Baird et al. 2014).

Ganey et al. (2017) tested eight full-scale rocking walls under quasi-static, reversed-cyclic lateral loading. The walls had different initial PT forces, boundary conditions, layups (i.e., arrangement of CLT layers), and/or the use of UFPs as coupling devices. It was evident from results that uncoupled walls exhibited low overturning moment resistance and energy dissipation compared to walls coupled with UFPs. Subsequent shake table tests on a 2-story building with coupled PT CLT rocking walls were conducted by Pei et al (2018) to evaluate system performance under service level earthquake (SLE) (43-year return period), DE, and MCE_R earthquake demands. At MCE_R, inelastic response was limited to wall toes and UFP coupling devices, while gravity and diaphragm components exhibited no damage and PT rods exhibited minimal stress losses.

A mechanics-based analytical approach that does not require numerical modeling to predict the force-deformation response of a coupled CLT rocking wall system was developed by Jin et al. (2019). The backbone curve of the CLT rocking wall system derived using the analytical methods developed by Jin et al. (2019) compared well to those computed using nonlinear finite element models developed in the program SAP2000 (CSI 2010). The extent of plasticity at the base of the wall is not assessed in this approach. Numerical models for PT CLT rocking walls were developed by Ganey (2015) and Kovacs and Wiebe (2017) in the structural analysis program OpenSees (Mazzoni et al. 2006). These models consist of distributed springs, characterized with an idealized, bilinear, elastic-plastic behavior of CLT in compression at the base of the wall panel that capture the spread of plasticity along the base of the wall. Ganey (2015) and Kovacs and Wiebe (2017) compared their model results to test results from Ganey (2015) and Sarti et al (2016a), respectively. Wilson et al. (2019) formulated finite element models using SAP2000 (CSI 2010) that enabled determination of the horizontal spread of plasticity along the base of the wall in addition to the vertical spread of plasticity up the height of the wall. To address the lack of computational efficiency in using the finite element model for NLTH analysis, Wilson et al. (2019) provided a procedure to formulate a lumped plasticity model for a wall, based on results from a pushover analysis of the more-refined finite element model. Results from both the finite element and lumped plasticity models matched reasonably well with experimental results from Ganey et al. (2017). The lumped plasticity model is computationally efficient for NLTH analysis and was used in this study for NLTH analysis.

NLTH analysis investigations of PT CLT rocking wall buildings have been conducted on midrise, two-dimensional (2D) building models in OpenSees (Mazzoni et al. 2006) by Ganey (2015) and Kovacs and Wiebe (2017) using the distributed spring models previously described. Utilizing a symmetrical, rectangular building layout, Ganey (2015) considered 8-story and 14-story buildings subjected to far-field ground motions scaled to represent SLE, DE, and MCE_R intensity levels in regions with high seismic accelerations under stiff soil conditions (Site Class D). Single rocking stories were considered at different building elevations, while the remaining stories utilized CLT walls with hold-down anchorages. Kovacs and Wiebe (2017) investigated the response of a symmetrical, square, 6-story PT CLT rocking wall building with synthetic far-field and near-fault ground motions representative of low-to-moderate seismic accelerations in regions with very dense soil (Site Class C). Walls were located around the exterior and central core of the building, and the estimated fundamental period was 1.8 s. Both of these studies focused on midrise building(s) without inclusion of high acceleration, near-fault ground motions. The focus of this paper is a three-dimensional (3D) NLTH analysis of both a 5-story and 12-story prototype building assumed to be located in Seattle, Washington, on a Site Class D location, with the use of both far-field and near-fault ground motions scaled to DE and MCE_R intensity levels.

Building Design 180

This section presents the design methodology for the two prototype buildings used in this study, while the following section describes their final design and dynamic characteristics. The low-rise building, shown in Fig. 1(a), was a 5-story office building with a total height of 19.8 m and a floor-to-floor height of 4 m, while the midrise building, shown in Fig. 1(b) was a 12-story residential building with a total height of 45.7 m, and a floor-to-floor height of 3.8 m. The low-rise building had six and four rocking wall lines in the North-South (N-S) and East-West (E-W) directions, respectively. The midrise building had eight wall lines in both directions. Each wall line consisted of three wall segments coupled with UFPs. Two UFPs were placed between two wall segments on a given floor, resulting in four UFPs on a given wall line for a single floor, as

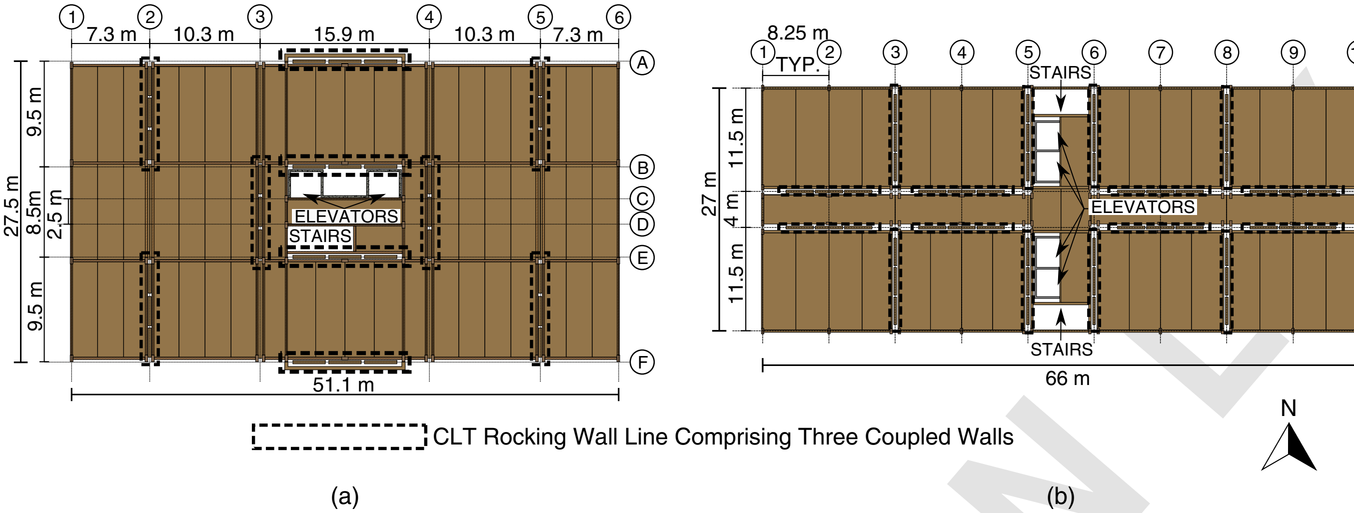

Fig. 1. Floor plan for: (a) low-rise building; and (b) midrise building.

indicated in Fig. 3. More walls were used in the taller building to satisfy the strength and drift demands. Gravity loading was not transferred to the walls and was carried solely by an independent glued-laminated timber (GLT or glulams) framing system. The two buildings were classified as Risk Category II (ICC 2018) and were assumed to be located at an arbitrary site in Seattle, with Site Class D soil conditions. It was assumed that foundations, collectors, and diaphragm-to-wall connections remained elastic under all demand levels. CLT diaphragm panels were assumed to remain elastic, with panel-to-panel connections within the diaphragm assumed to be rigid against deformation.

Preliminary gravity design was conducted to approximate member sizes and estimate building weight. It was assumed all elements were simply supported and beam elements were fully braced against lateral torsional buckling. Superimposed dead loads were assumed, while live and snow loads were determined in accordance with ASCE 7-16 (ASCE 2017). Utilizing the gravity loads in Table 1 and the Load and Resistance Factor Design (LRFD)

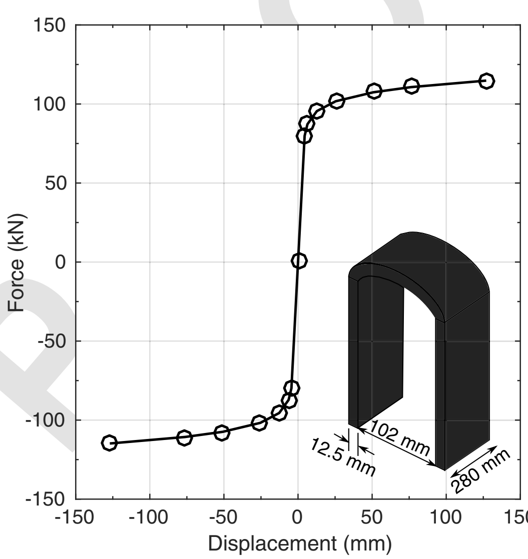

Fig. 2. UFP dimensions (not to scale) and associated Ramberg-Osgood computed backbone curve.

methodology, the governing member sizes of the floor system and their associated material specifications, provided in Table 2, were determined using E-1.8E class glulams and following the design procedures provided by the American Wood Council (AWC) (2017), which are similar, if not identical, in how beam and diaphragm theory is applied in the design standards in most countries around the world. Diaphragms and walls were designed to remain elastic, with stiffness methods being used to distribute the loads to the walls. The mechanical properties used for design are provided in Tables 2 and 5.

Wind loads were computed in accordance with the directional procedure in ASCE 7-16 (ASCE 2017) using a wind speed (V) of 97 mph for Seattle, directionality factor (K_d) of 0.85, exposure category of B, topographic factor (K_{zt}) of 1.0, gust effect factor (G) of 0.85, and enclosed building envelope. The computed maximum over turning moment at the base due to wind loading in the N-S and E-W directions was 8,532 and 4,180 kN · m, respectively, for the low-rise building and 75,050 and 28,000 kN · m, respectively, for the midrise building. An initial PT force, provided in Table 3, was selected so that the decompression moment of the walls was greater than the wind load overturning moment, keeping the system response linear elastic under the design wind demand. All UFPs remained elastic under all load levels up to the decompression state, and this was checked with pushover analysis.

Seismic performance objectives for both buildings were established for DE and MCE$_R$ intensity levels. With the exception of the UFPs and wall toes, all components were designed to remain elastic at both intensity levels. All wall toes at ground level and UFPs throughout the building were designed to exhibit inelastic response at DE intensities. These performance objectives are consistent with those assumed by Ganey (2015), except for the allowance of wall toe crushing at DE level events to increase energy dissipation.

Lateral demands were estimated for both buildings using the response spectrum parameters presented in Table 4 in conjunction with the equivalent lateral force (ELF) procedure in ASCE 7-16 (ASCE 2017). To conduct the initial ELF procedure to estimate the required size and number of walls, a value for R of six was assumed for PT CLT rocking walls, which was consistent with the value assumed by Ganey (2015) for PT CLT rocking walls and lower than the value of seven recommended by Sarti et al. (2017) for PT LVL rocking walls. Low- and midrise building weights were estimated to be approximately 19,260 and 65,830 kN, respectively.

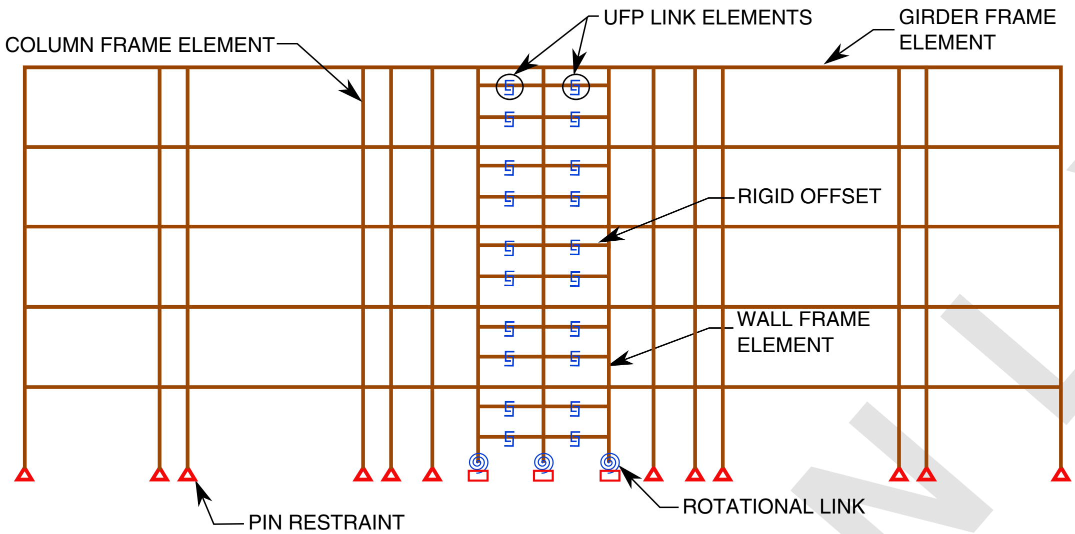

F3:1 **Fig. 3.** Elevation profile of low-rise building.

Table 1. Gravity loads for low-rise building and midrise building

	Loading	Location	Building	Object/value
T1:1	Loading	Location	Building	Object/value
T1:2	Dead loads	Roof	LR[a]	MEP/Misc.: 0.5 kPa
T1:3			MR	MEP/Misc.: 1.0 kPa
T1:4		Floors	LR, MR	MEP/Misc.: 1.0 kPa
T1:5		Exterior	LR, MR	Cladding: 0.75 kPa
T1:6	Live loads	Roof	LR, MR	Live Roof: 1.0 kPa
T1:7		Floors	LR	Offices: 2.4 kPa
T1:8			MR	Residential: 1.9 kPa
T1:9			LR, MR	Lobby: 4.8 kPa
T1:10	Snow loads	Roof	LR, MR	1.2 kPa (min)[a]

Note: LR = low-rise building; and MR = midrise building.
[a]Minimum snow load for city of Seattle.

The computed base shear and overturning moment demands for the low-rise building were 2,896 kN and 39,996 kN · m, respectively, while demands for the midrise building were 5,235 kN and 164,415 kN · m, respectively.

Thick, 9-ply CLT wall panels were utilized in the buildings to ensure an elastic in-plane shear and flexural response was exhibited above the toe crushing region of the wall at DE and MCE_R intensities. PT rods were designed to remain elastic up to a first story drift magnitude of 5%, which is larger than ASCE 7-16 code acceptable DE and MCE_R drift magnitudes of 2% and 4%, respectively. The toe crushing resistance of the wall panels was determined using expected material properties, rather than allowable properties. UFPs were designed with a low yield displacement and force, relative to possible UFP configurations (Baird et al. 2014), to ensure all UFPs throughout the building yielded at DE and MCE_R intensities.

The design procedure used to determine the lateral system parameters of both buildings presented in Table 4 is summarized in the remainder of this section. The shear resistance of the lateral system was determined using the cumulative, allowable in-plane shear strength (341.8 kN/m) of all CLT wall panels, and determined based on values provided in Structurlam (2016). The inelastic overturning moment resistance was determined using the equation from Ganey (2015)

$$M = \sum_{1}^{n_w} (T + W)d + \sum_{1}^{n_{ufp}} V_{UFP} L_W \qquad (1)$$

where M is the total inelastic overturning moment resistance of the system, considering all walls in a given orthogonal direction at a given rocking interface (n_w) subjected to a prescribed rotation at the base, T is the tension force exhibited by the PT rods, W is the self-weight of the wall panels, d is the couple arm between T and the

Table 2. Material specifications and sizes of gravity system elements

	Building	Component	Material description	Size/description
T2:1	Building	Component	Material description	Size/description
T2:2	Low-rise	Floor panels	SPF, No.2 and Btr., V2M1.1[a]	5-Ply (175-mm depth)
T2:3		Beams	DFL, 24F-1.8E	310 × 488 mm
T2:4		Girders	DFL, 24F-1.8E	310 × 712 mm
T2:5		Columns	DFL, V3	310 × 338 mm
T2:6	Midrise	Floor panels	SPF, No. 2 and Btr., V2M1.1[a]	5-Ply (175-mm depth)
T2:7		Beams	DFL, 24F-1.8E	310 × 450 mm
T2:8		Girders	DFL, 24F-1.8E	310 × 875 mm
T2:9		Columns (stories 1–4)	DFL, V4	310 × 525 mm
T2:10		Columns (stories 5–8)	DFL, V4	310 × 375 mm
T2:11		Columns (stories 9–12)	DFL, V4	225 × 300 mm

Note: SPF = spruce-pine-fir; and DFL = Douglas-fir-larch.
[a]Layup classification corresponding to Structurlam (2016).

Table 3. Lateral system parameters for low-rise building and midrise building

Parameter	Low-rise building	Midrise building
Wall segment length (m)	2.75 (N-S), 3 (E-W)	3 (N-S, E-W)
Wall thickness (mm)	315 (9-ply)	315 (9-ply)
Initial PT force (kN)	530	1,800
PT bar diameter (mm)	45	45
Number of PT rods per panel	4	4
Total number of wall segments	18 (N-S), 12 (E-W)	24 (N-S, E-W)
Total number of UFPs	120 (N-S), 80 (E-W)	768 (N-S, E-W)

Table 4. Response spectrum parameters

Design parameter	Parameter value
Building location	Latitude: 47.622°
	Longitude: −122.336°
Importance factor (I_e)	1.0
Mapped spectral	S_s: 1.374 g
Response parameters	S_1: 0.478 g
Site class	D
Design spectral	S_{DS}: 1.099 g
Acceleration parameters	S_{D1}: 0.581 g
Seismic design category	D

resultant compression force at the toe, n_{ufp} is the number of UFPs utilized within the system, V_{UFP} is the shear resistance of a UFP, and L_w is the length of a wall panel. The dead load does not affect the overturning calculation because the connection to transfer the lateral loads to the walls is slotted to eliminate any gravity loads being transferred to the walls. The gravity loads are resisted by an independent beam-column structural system. The cross-sectional analysis procedure, modified by and explained in Ganey (2015) for PT CLT rocking walls, was used to determine T and d. The shear resistance of a single UFP was computed using the equation from Baird et al. (2014)

$$F_y = \frac{f_y b_u t_u^2}{2D_u} \tag{2}$$

where F_y is the effective yield force of the UFP, f_y is the yield strength of the steel, b_u is the width of the UFP, t_u is the thickness of the UFP, and D_u is the inner diameter of the UFP. The following equations from Baird et al. (2014) were used to determine the backbone curve of the UFPs:

$$\delta = \frac{F}{k_0}\left[1 + \left(\frac{F}{F_y}\right)^{r-1}\right] \tag{3}$$

$$k_0 = \frac{16Eb_u}{27\pi}\left(\frac{t_u}{D_u}\right)^3 \tag{4}$$

$$r = 7.1ln\left(\frac{t_u}{D_u}\right) + 29.5 \tag{5}$$

where δ is the UFP displacement; F is the corresponding force, k_0 is the initial stiffness of the UFP, and r is the Ramberg-Osgood factor. Baird et al. (2014) showed that Eqs. (3)–(5) accurately predict the backbone curve of various UFP designs. By iterating for F in Eq. (3), the backbone relationship of the UFP used in the buildings with b_u, t_u, and D_u dimensions of 279.4, 12.7, and 101.6 mm, respectively, were determined, as illustrated in Fig. 2.

A sufficient number of walls and UFPs were incorporated into both buildings to meet seismic strength demands. Additional UFPs were incorporated to stiffen the system and ensure code acceptable interstory drift magnitudes that did not exceed 2% and 4% for DE and MCE_R level events, respectively.

Due to the low flexural stiffness of the PT CLT system, the use of a single rocking joint at the base of the wall was not sufficient for the midrise building because the interstory drifts at upper stories exceeded code acceptable levels. Therefore, a second rocking joint was incorporated at Level 7 (50% of building height) to reduce wall flexural demands in the lower stories, resulting in smaller upper floor displacements to meet interstory drift requirements. Several previous studies have investigated segmented structural systems using rocking walls or seismic isolation to reduce flexural demands along the height of the building and to better account for higher mode effects on structural response (Chey et al. 2010; Panagiotou and Restrepo 2009; Wiebe et al. 2013a, b). Particularly relevant to this study are prior computational studies (Wiebe and Christopoulos 2010; Li et al. 2017) that investigated the effect and optimal location of second rocking joints, which were found to decrease the higher mode effects, reduce interstory drifts, and reduce flexural demand along the height of the structure. Li et al. (2017) determined that the optimum location of a second rocking joint was between 22% and 53% of the height using three prototype buildings (9-, 20-, and 30-story) and a suite of 20 ground motions. Wiebe and Christopoulos (2010) concluded that the maximum flexural demand on the system decreased significantly when a second rocking joint was implemented within the lower half of the building. The authors are not aware of any published studies on the behavior of segmented PT CLT rocking walls with a second rocking joint.

Building Model Characterization

Building models, constructed in SAP2000 (CSI 2010), included both the lateral and gravity system, as shown in Fig. 3, to accurately distribute building mass and capture torsional building response. Elastic frame elements were used for gravity components and were characterized with the material properties and section characteristics specified in Table 2. Elastic shell elements, capable of capturing shear deformation, were utilized for the CLT diaphragms and were characterized with the material properties in Table 2. Shell elements were rigidly connected, constrained to their adjacent girder elements, and made rigid out-of-plane to avoid undesirable modes and the need for supporting beams within the model. Coupled rocking walls utilized the reduced-order modeling approach described in Wilson et al. (2019), with the system parameters and material properties in Tables 4 and 5, respectively, as well as the UFP backbone curve shown in Fig. 2 for the inelastic shear link with a kinematic hardening relationship. Each wall element was connected to the diaphragms through an elastic shear link element that transferred lateral loads.

The midheight rocking joint at Level 7 of the midrise building was modeled as shown in Fig. 4. A rigid frame element rested on two vertical restraints that allowed horizontal translation and rotation about all three axes. Shear continuity between wall elements above and below the joint was provided with a shear link element, while moment demands from the reduced-order model springs were directly transferred into the rigid girder, resulting in no moment transfer across the joint.

Table 5. Material characteristics for high-order and reduced-order models

Material	CLT								PT Rod		UFP
Property	E_1 (MPa)	E_2 (MPa)	E_3 (MPa)	G_1 (MPa)	G_2 (MPa)	G_3 (MPa)	$\nu_{1,2,3}$	f_y (MPa)	E (MPa)	f_y (MPa)	f_y (MPa)
Value	4,215	5,270	937	219	173	443	0.3	37	200,000	882	413

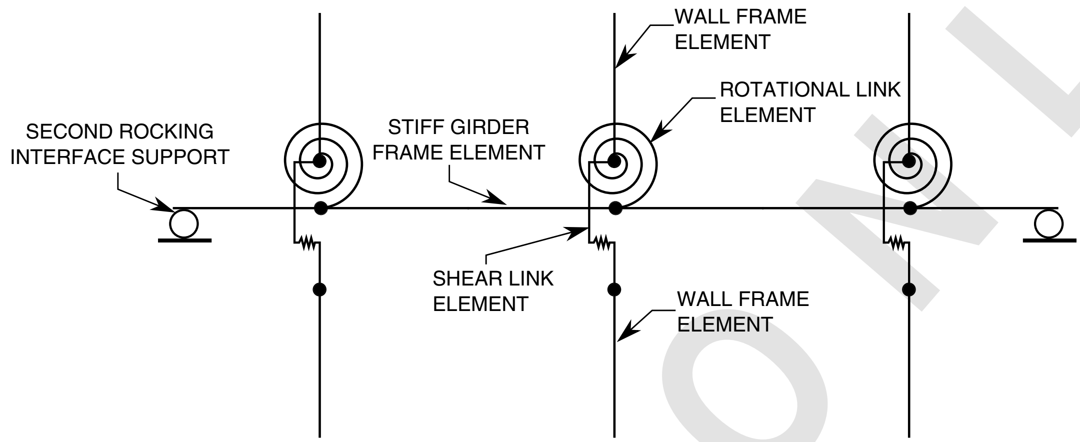

Fig. 4. Midheight rocking joint modeling schematic.

Member self-weight, superimposed dead (including that of the unincorporated interior beams) and live loads on the diaphragms, and cladding line dead loads along the perimeter framing were included in the model, with the values used provided in Table 1. NLTH analysis included the total dead load and 20% of the live load, consistent with ASCE 7-16 (ASCE 2017). For near-fault motions, fault-perpendicular orientation was assumed to run parallel with the N-S direction of each building. A proportional mass and stiffness damping value of 1% of critical was applied to the building modes that contributed a total of at least 90% modal mass participation in each principle building direction, which were the first five and six modes determined from eigenvalue analysis for the low- and midrise building, respectively. The modal mass participation and period for each of these modes is provided in Table 6. Newmark time-stepping integration with constant acceleration parameters was utilized for all time-history analyses.

Table 6. Modes summing to at least 90% modal mass participation for low-rise building and midrise building

Building	Mode	Period (s)	Mass participation (%)	Description
Low-rise	1	1.06	84	E-W translation mode 1
	2	0.94	82	N-S translation mode 1
	3	0.92	2	Torsion mode 1
	4	0.3	9	E-W translation mode 2
	5	0.27	8	N-S translation mode 2
Midrise	1	3.36	2	Torsion mode 1
	2	2.14	86	E-W translation mode 1
	3	2.13	86	N-S translation mode 1
	4	1.06	2	Torsion mode 2
	5	0.68	6	N-S translation mode 2
	6	0.67	6	E-W translation mode 2

Nonlinear Time-History Analysis Evaluation

Ground Motions

All far-field (FF), near-fault with no pulse (NFNP), and near-fault with pulse (NFP) ground motions used were described in FEMA P-695 (ATC 2009) and were obtained from the PEER NGA-West 2 ground motion database. Response spectra for each ground motion were developed in accordance with ASCE 7-16 (ASCE 2017) for 5% damping. All ground motions of a specific type were scaled to DE and MCE_R in accordance with the amplitude scaling procedure described in Chapter 16 of ASCE 7-16, which specifies scaling over a range of period values. The mean, scaled, maximum direction response spectrum for each ground motion type is illustrated in Fig. 5 for both buildings. Using the analysis results, both buildings were assessed with respect to wall shear and moment resistance, interstory drift, crushing at the wall toes, and the vertical deformation of the UFPs.

Low-Rise Building Analysis Results

The maximum in-plane shear resistance exhibited at MCE_R in the North-South (N-S) (fault-perpendicular) and East-West (E-W) (fault-parallel) direction was 454 and 543 kN, respectively. These values are well below the allowable in-plane shear strength of 939 and 1,041 kN for the 2.75-m and 3-m wall lengths, respectively, determined based on the strength per unit length of 341.84 kN/m provided by Structurlam (2016). The mean peak in-plane flexural demands on the rocking wall panels for all ground motion types at DE and MCE_R level events are provided in Figs. 6(a and b) for the N-S and E-W directions, respectively. At the base of the wall panels, NFP ground motions produced the highest flexural demands of 1,479 and 2,011 kN · m for DE and MCE_R level events, respectively. Above the base in the N-S direction, FF ground motions resulted in the largest flexural

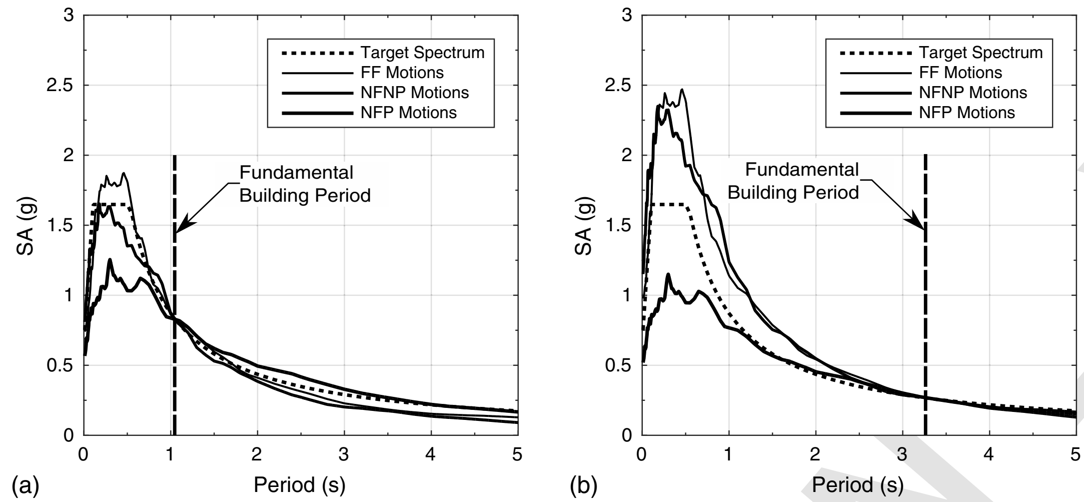

Fig. 5. Scaled ground motion mean spectra and target spectrum for: (a) low-rise building; and (b) midrise building.

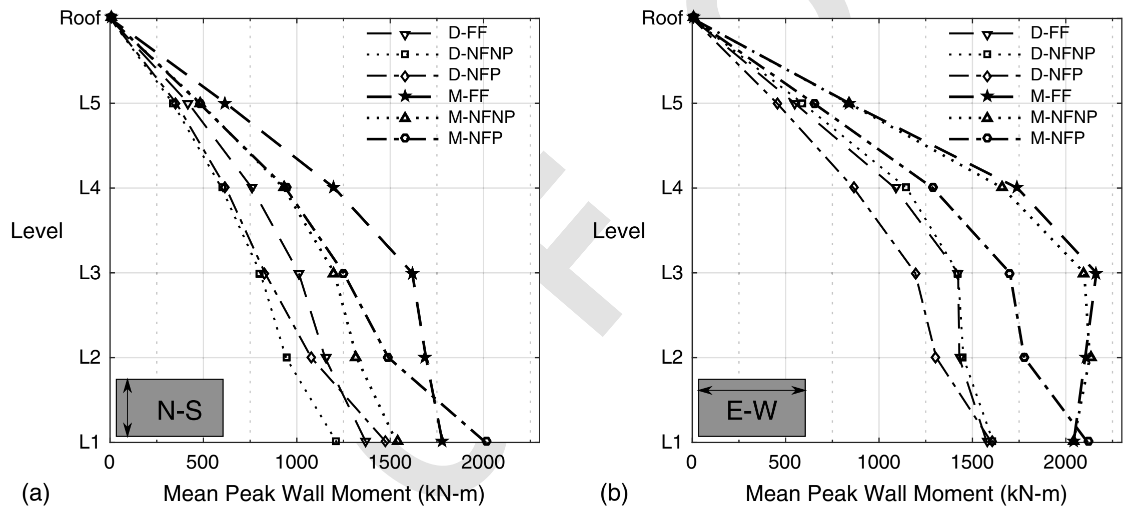

Fig. 6. Low-rise building mean peak wall moment response for all ground motion types scaled to DE and MCE_R level intensities in: (a) North-South (N-S); and (b) East-West (E-W) direction.

demands. In the E-W direction, FF and NFNP ground motions produced similar results at both intensity levels, with a maximum moment of 1,613 $kN \cdot m$ at the base and 2,164 $kN \cdot m$ at Level 3 for DE and MCE_R level events, respectively. By utilizing the allowable design values in Structurlam (2016), the in-plane flexural strength of the 2.75-m and 3-m wall panel was computed to be 3,808 and 4,701 $kN \cdot m$, respectively, which exceeded the demands illustrated in Fig. 6, indicating an elastic flexural response of the wall panels (excluding nonlinearity at the toe).

The mean peak interstory drift demands for DE and MCE_R level events in the N-S and E-W direction for the low-rise building are illustrated in Figs. 7(a and b), respectively. The interstory drift was computed in accordance with ASCE 7-16 (ASCE 2017) using nodes located at the building corners on each floor. Ground motion types scaled to a specific intensity level (DE or MCE_R) in the E-W direction exhibited more consistent behavior between one another relative to the N-S direction. NFP ground motions acting in the N-S direction resulted in the largest interstory drift magnitudes of 1.17% and 1.95% at DE and MCE_R level events, respectively. Since the fundamental period of the low-rise building fell within the velocity-sensitive range of the target spectrum, it was expected that NFP ground motions would produce the highest interstory drifts in the direction subjected to the characteristic velocity pulse. Considering both principle directions, the maximum interstory drifts exhibited at DE and MCE_R level events were well below the ASCE 7-16 (ASCE 2017) drift limits of 2% and 4%, respectively, indicating code compliance with respect to drift.

The high-order wall model described by Wilson et al. (2019), which considered elastic-perfectly plastic behavior of CLT in compression, was used to determine the amount of inelastic (damaged) area at the toe of the CLT rocking walls. This was accomplished by subjecting the high-order model to a lateral displacement equal to that of the reduced-order model used in the NLTH analyses. The damaged material at the wall corners formed roughly a rectangle with mean peak width (b) and height (h) provided in Table 7. For both DE and MCE_R level events, NFP ground motions produced the highest inelastic response at the toe in the N-S direction with an approximated peak in elastic width and height of 40 and

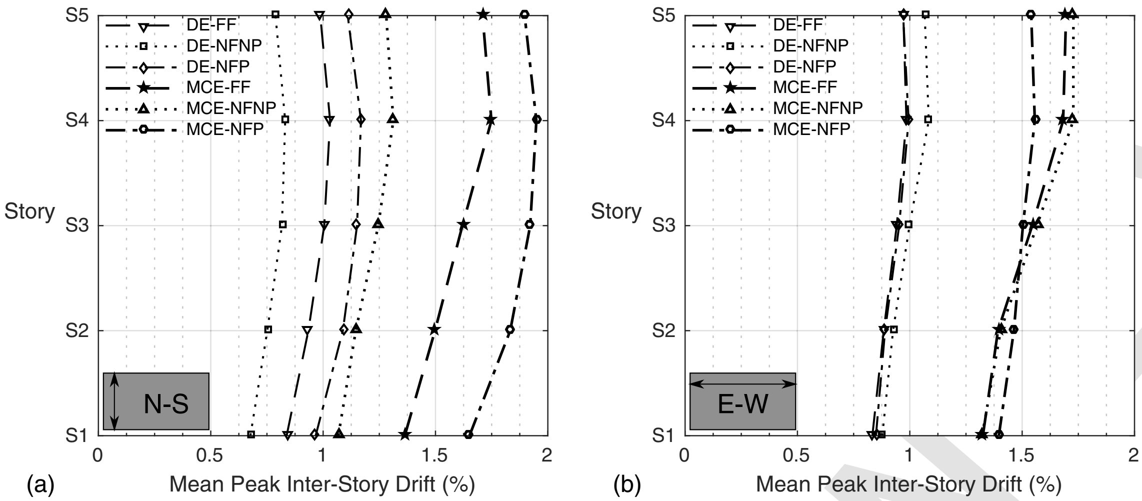

Fig. 7. Low-rise building mean peak interstory drift response for all ground motion types scaled to DE and MCE_R level intensities in: (a) North-South (N-S); and (b) East-West (E-W) direction.

Table 7. Damaged wall toe dimensions for low-rise building

	N-S			E-W		
	FF	NFNP	NFP	FF	NFNP	NFP
Design level (DE) earthquake						
b (mm)	30	20	40	25	40	30
h (mm)	40	30	60	35	70	50
Maximum considered earthquake (MCE_R)						
b (mm)	70	45	80	70	80	85
h (mm)	100	70	140	90	110	135

60 mm, respectively, considering all ground motions. In the E-W direction, NFNP and NFP ground motions produced the maximum in elastic response for DE and MCE_R level events, respectively. Since crushing at the toes is directly related to the moment demand at the base, peak crushing deformation in both directions occurred for the ground motion that created peak moment demand at the base of the wall panels. All ground motion types resulted in inelastic behavior at the base for DE level events, with greater inelastic strains and volumes for the MCE_R level events, consistent with the performance objectives of this study.

The mean peak vertical deformations exhibited by the UFPs (D_x) normalized to the yield displacement of the UFPs (D_y) for both DE and MCE_R level events are shown for the N-S and E-W direction in Figs. 8(a and b), respectively. UFPs located higher from the base of the wall experience larger deformation demand than those closer to the base of the wall in both directions for all ground motion types. Since all wall panels were continuous, i.e., without rocking joints, between floors in the low-rise building, the wall rotation increased with building height, imposing higher UFP deformation demand at the upper stories. Furthermore, the displacement demands imposed on all UFPs were well beyond yield displacement at DE level events and more so at MCE_R level events, consistent with the desired behavior outlined in the performance objectives.

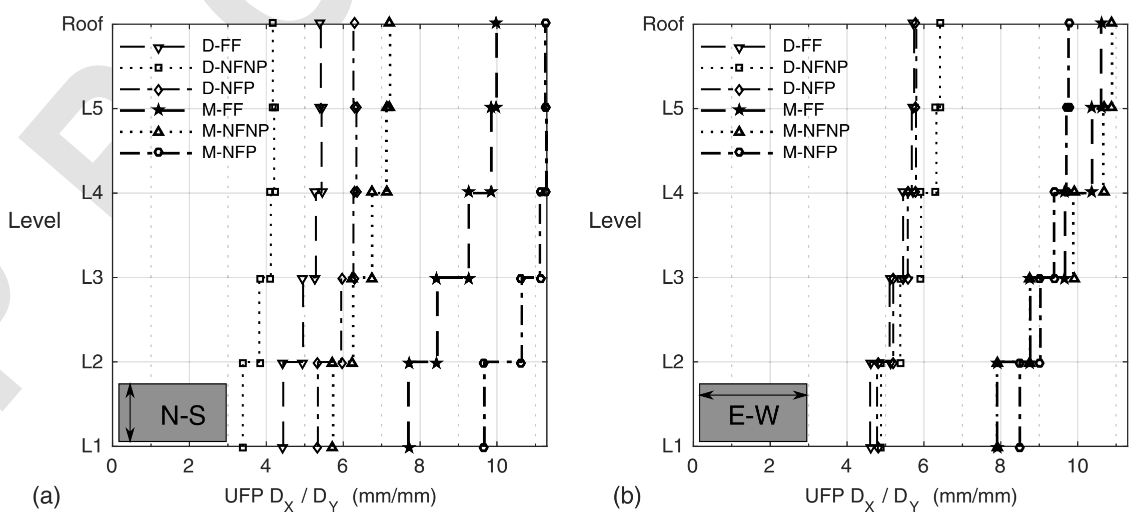

Fig. 8. Low-rise building mean peak UFP deformation response for all ground motion types scaled to DE and MCE_R level intensities in: (a) North-South (N-S); and (b) East-West (E-W) direction.

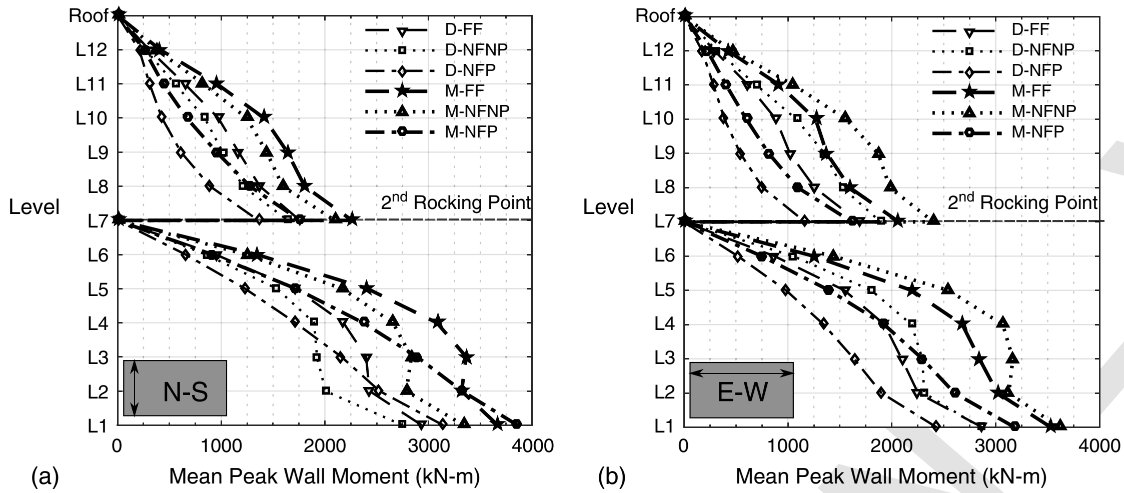

Fig. 9. Midrise building mean peak wall moment response for all ground motion types scaled to DE and MCE_R level intensities in: (a) North-South (N-S); and (b) East-West (E-W) direction.

Midrise Building Analysis Results

The maximum in-plane shear demands exhibited by the midrise building for MCE_R level events in the North-South (N-S) and East-West (E-W) directions were 603 and 614 kN, respectively. These values were well below the allowable in-plane shear strength of 1,041 kN determined based on unit strength values provided by Structurlam (2016), indicating an elastic shear response of the wall segments in both directions. The mean peak in-plane flexural demands exhibited at DE and MCE_R level events are shown in Figs. 9(a and b) in the N-S and E-W direction, respectively. The trends in the data in Fig. 9 suggest that the midheight rocking joint reduces flexural demands exhibited by walls at both rocking joints. In the N-S direction, near-fault with pulse (NFP) ground motions resulted in the highest flexural demands at the base rocking joint, while far-field (FF) and near-fault with no pulse (NFNP) resulted in larger flexural demand sat the midheight rocking joint. Flexural demands in walls above the midheight rocking joint were less sensitive to NFP ground motions than FF and NFNP ground motions. For MCE_R level events, the maximum in-plane flexural demands exhibited at the base rocking joint in the N-S and E-W directions were 3,857 and 3,610 $kN \cdot m$, respectively, while walls attached to the midheight rocking joint exhibited demands of 2,263 and 2,400 $kN \cdot m$, respectively. The results obtained from this study are similar to results reported by Wiebe and Christopoulos (2009) in that the implementation of the second rocking joint reduced the moment demand on walls above and below the second rocking joint. All demands were well below the allowable in-plane flexural strength of 4,701 $kN \cdot m$ provided by Structurlam (2016), indicating an elastic flexural response (with the exception of the toe).

The mean peak interstory drift demands for the midrise building at both DE and MCE_R level events in the N-S and E-W direction are provided in Figs. 10(a and b), respectively. The interstory drift demands in stories above the midheight rocking joint were significantly lower than the stories below due to the lower flexural demands on the walls. In the N-S direction, both FF and NFP ground motions at DE and MCE_R level intensities generated larger interstory drift demands than NFNP ground motions for stories below the midheight rocking joint. However, interstory drift demands for NFP motions decreased for stories above the midheight rocking

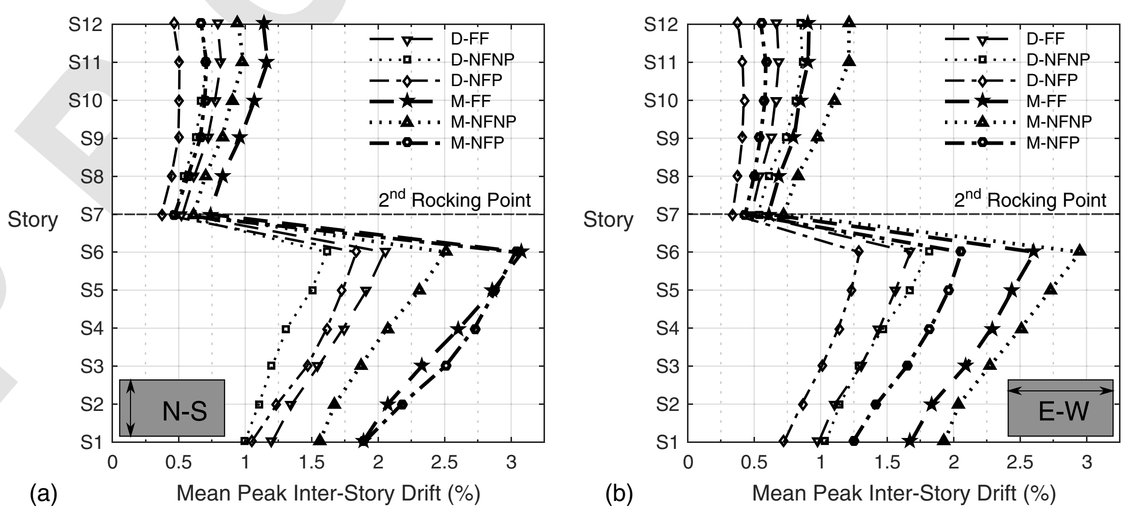

Fig. 10. Midrise building mean peak interstory drift response for all ground motion types scaled to DE and MCE_R level intensities in: (a) North-South (N-S); and (b) East-West (E-W) direction.

Table 8. Damaged wall toe dimensions for midrise building

	N-S			E-W		
	FF	NFNP	NFP	FF	NFNP	NFP
DE base rocking joint						
b (mm)	55	65	65	60	70	50
h(mm)	75	100	105	110	100	65
MCE_R base rocking joint						
b (mm)	75	90	120	85	100	75
h (mm)	115	145	160	115	130	125
MCE_R midheight rocking joint						
b (mm)	30	0	0	20	40	0
h (mm)	50	0	0	30	65	0

joint relative to stories below the midheight rocking joint. Considering both directions, the maximum interstory drift demands were 2.04% and 3.08% for DE and MCE_R level events, respectively, in stories below the midheight rocking joint, and 0.82% and 1.17% for DE and MCE_R level events, respectively, in stories above the midheight rocking joint. A total of 20 out of 22 FF ground motions did not produce peak story drifts that exceeded 2% at DE level events, while no ground motions produced peak story drifts that exceeded 4% drift for MCE_R events.

The mean peak dimensions of timber at the toes that exhibited an inelastic response, determined from the high-order model, for all ground motion types and for both DE and MCE_R at both rocking joints are given in Table 8. In the N-S direction, NFP ground motions led to the greatest amount of inelasticity at the base for both DE and MCE_R level events. In the N-S direction for NFP ground motions at DE level events, walls at the base rocking joint experienced 65 and 105 mm of inelastic response along the base and height of the wall, respectively. Inelastic behavior for DE level events did not occur at the midheight rocking joint, while select ground motion types caused inelastic response at MCE_R level events. The crushing behavior for walls at the base rocking joint were consistent with the performance objectives outlined in this study.

The mean peak UFP deformation demands normalized to the yield displacement for DE and MCE_R level events are provided in Figs. 11(a and b) for the N-S and E-W direction, respectively. The low flexural demands for walls above the midheight rocking joint resulted in smaller interstory drift demands, which resulted in much lower UFP deformations above the midheight rocking joint. For MCE_R level events, NFP motions caused the largest UFP deformations below the midheight rocking joint in the N-S direction, while FF events caused the largest deformations above the midheight rocking joint for all intensity levels.

Summary and Conclusions

Nonlinear time history analyses were conducted for a low-rise, 5-story office building and a midrise, 12-story residential building that both utilized post-tensioned (PT) cross-laminated timber (CLT) rocking walls coupled with U-shaped flexural plate (UFP) hysteretic damping devices as the sole lateral force resisting system. Both buildings were designed to meet performance objectives that limited structural damage to crushing at the wall toes and nonlinear deformation in the UFPs, while ensuring ASCE 7-16 DE and MCE_R interstory drift limits were satisfied and the post-tensioned rods remained linear for all demands. The 12-story building possessed a second rocking joint at Level 7 (i.e., midheight) to mitigate higher mode effects, reduce wall flexural demands, and meet code acceptable drift levels. The building models incorporated newly developed modeling methods for PT CLT rocking walls to investigate in-plane wall shear and flexural demands, interstory drift demand, crushing at the wall toes, and vertical UFP deformation. A total of 50 ground motions, consisting of far-field and near-fault events, with and without pulses, were applied to both building models at DE and MCE_R intensities to conduct nonlinear time-history analyses. The main conclusions resulting from this study are:

- Both the low-rise and midrise buildings were able to meet the performance objectives, the ASCE 7-16 interstory drift limits, and the allowable in-plane wall shear and flexural strength requirements at both DE and MCER intensity levels.
- The response of the low-rise building was more sensitive to ground motion pulses than the midrise building, resulting in larger wall moment demand, interstory drift demand, crushing at the wall toes, and UFP deformation. This sensitivity was attributed to the velocity-sensitive correlation of the building period to the target response spectrum. This sensitivity was also attributed to the midheight rocking joint in the midrise building,

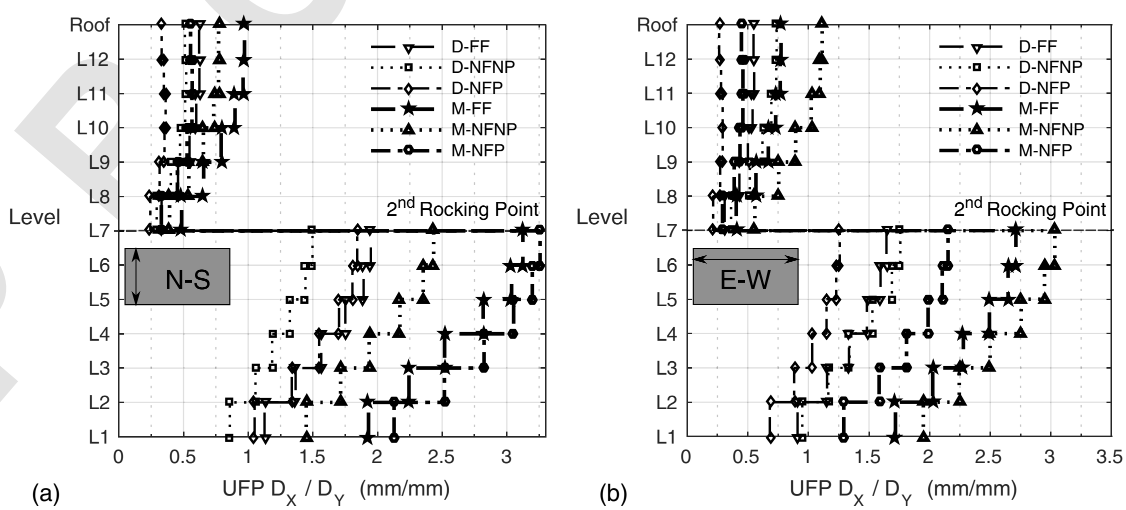

Fig. 11. Midrise building mean peak UFP deformation response for all ground motion types scaled to DE and MCE_R level intensities in: (a) North-South (N-S); and (b) East-West (E-W) direction.

which minimized the directivity effects of near-fault motions above the midheight rocking joint.

- Walls in the low-rise building exhibited a maximum plastic response at the toes of 80 and 140 mm along the base and height of the wall, respectively, while walls in the midrise building exhibited a maximum plastic response at the toes of 120 and 160 mm along the base and height of the wall, respectively, for MCER level events. These values indicate that wall damage is limited and localized at the wall toes.
- Maximum UFP deformation increased as the location increased up the height of the low-rise building, resulting in more energy dissipation at the upper portions of the wall segments. In the midrise building, similar behavior was observed below the midheight rocking joint. Above the midheight rocking joint, a significant drop in maximum UFP deformation was observed due to decreased flexural demands.

Data Availability Statement

Some or all data, models, or code generated or used during the study are available from the corresponding author, Daniel Dolan, upon written request.

Acknowledgments

This work was supported by the National Science Foundation under Grant No. CMMI-1635156. Any opinions, findings, conclusions, and recommendations presented in this paper are those of the authors and do not necessarily reflect the views of the National Science Foundation.

References

Akbas, T., et al. 2017. "Analytical and experimental lateral-load response of self-centering posttensioned CLT walls." *J. Struct. Eng.* 143 (6): 04017019. https://doi.org/10.1061/(ASCE)ST.1943-541X.0001733.

ASCE. 2017. *Minimum design loads and associated criteria for buildings and other structures*. ASCE/SEI 7-16. Reston, VA: ASCE.

ATC (Applied Technology Council). 2009. *Quantification of building seismic performance factors*. Rep. No. P-695. Redwood City, CA: ATC.

AWC (American Wood Council). 2017. *National design specification for wood construction with commentary.* ANSI/AWC NDS 2018. Leesburg, VA: AWC.

Baird, A., T. Smith, A. Palermo, and S. Pampanin. 2014. "Experimental and numerical study of U-shape flexural plate (UFP) dissipators." In *Proc., 2014 NZSEE Conf. New Zealand*.

Chey, M. H., G. Chase, J. B. Mander, and A. J. Carr. 2010. "Semi-active tuned mass damper building systems: Application." *Earthquake Eng. Struct. Dyn.* 39 (1): 69–89.

Chopra, A. 2012. *Dynamics of structures: Theory and applications to earthquake engineering*. 4th ed. Englewood Cliffs, NJ: Prentice Hall.

CSI (Computers and Structures Inc). 2010. *CSI analysis reference manual: For SAP2000, ETABS, SAFE and CSI Bridge*. Berkeley, CA: Computers and Structures.

Ganey, R. 2015. "Seismic design and testing of rocking cross laminated timber walls." M.S. thesis, Univ. of Washington.

Ganey, R., J. Berman, T. Akbas, S. Loftus, J. D. Dolan, R. Sause, J. Ricles, S. Pei, J. V. D. Lindt, and H.-E. Blomgren. 2017. "Experimental investigation of self-centering cross-laminated timber walls." *J. Struct. Eng.* 143 (10): 04017135. https://doi.org/10.1061/(ASCE)ST.1943-541X.0001877.

Holden, T., J. Restrepo, and J. B. Mander. 2003. "Seismic performance of precast reinforced and prestressed concrete walls." *J. Struct. Eng.* 129 (3): 286–296. https://doi.org/10.1061/(ASCE)0733-9445(2003)129:3(286).

ICC (International Code Council). 2018. *International building code*. IBC 2018. Country Club Hills, IL: ICC.

Jin, Z., S. Pei, H. Blomgren, and J. Powers. 2019. "Simplified mechanistic model for seismic response prediction of coupled cross-laminated timber rocking walls." *J. Struct. Eng.* 145 (2): 04018253. https://doi.org/10.1061/(ASCE)ST.1943-541X.0002265.

Kovacs, M., and L. Wiebe. 2017. "Controlled rocking CLT walls for buildings in regions of moderate seismicity: Design procedure and numerical collapse assessment." *J. Earthquake Eng.* 23 (5), https://doi.org/10.1080/13632469.2017.1326421.

Kurama, Y., S. Pessiki, R. Sause, and L. Lu. 1999a. "Seismic behavior and design of unbonded post-tensioned precast concrete walls." *PCI J.* 44 (3): 72–89. https://doi.org/10.15554/pcij.05011999.72.89.

Kurama, Y., R. Sause, S. Pessiki, and L.-W. Lu. 1999b. "Lateral load behavior and seismic design of unbonded post-tensioned precast concrete walls." *ACI Struct. J.* 96 (4): 622–632.

Kurama, Y. C. 2002. "Hybrid post-tensioned precast concrete walls for use in seismic regions." *PCI J.* 47 (5): 36–59. https://doi.org/10.15554/pcij.09012002.36.59.

Li, T., J. W. Berman, and R. Wiebe. 2017. "Parametric study of seismic performance of structures with multiple rocking joints." *Eng. Struct.* 146 (Sep): 75–92. https://doi.org/10.1016/j.engstruct.2017.05.030.

Mazzoni, S., F. McKenna, M. H. Scott, and G. L. Fenves. 2006. *OpenSEES command language manual*. Berkeley, CA: Pacific Earthquake Engineering Research Center.

Nakaki, S. D., J. F. Stanton, and S. Sritharan. 1999. "An overview of the PRESSS five-story precast test building." *PCI J.* 44 (2): 26–39. https://doi.org/10.15554/pcij.03011999.26.39.

Panagiotou, M., and J. I. Restrepo. 2009. "Dual-plastic hinge design concept for reducing higher-mode effects on high-rise cantilever wall buildings." *Earthquake Eng. Struct. Dyn.* 38 (12): 1359–1380. https://doi.org/10.1002/eqe.905.

PEER (Pacific Earthquake Engineering Research Center). 2017. *Tall buildings initiative: Guidelines for performance-based seismic design of tall buildings*. 2.0 ed. Berkeley, CA: PEER.

PEER (Pacific Earthquake Engineering Research Center). 2018. "PEER ground motion database." Accessed May 2018. https://ngawest2.berkeley.edu.

Pei, S., J. Van De Lindt, A. Barbosa, J. Berman, E. McDonnell, J. Dolan, R. Zimmerman, R. Sause, J. Ricles, and K. Ryan. 2018. "Full-scale shake table test of mass-timber building with resilient post-tensioned rocking walls." In *Proc., 2018 World Conf. of Timber Engineering, Korea*.

Perez, F. J., S. Pessiki, and R. Sause. 2013. "Experimental lateral load response of unbonded post tensioned precast concrete walls." *ACI Struct. J.* 110 (6): 1045–1055.

Priestley, M. J. N., S. S. Sritharan, J. R. Conley, and S. Pampanin. 1999. "Preliminary results and conclusions from the PRESSS five-story precast concrete test building." *PCI J.* 44 (6): 42–67. https://doi.org/10.15554/pcij.11011999.42.67.

Restrepo, J. I., and A. Rahman. 2007. "Seismic performance of self-centering structural walls incorporating energy dissipaters." *J. Struct. Eng.* 133 (11): 1560–1570. https://doi.org/10.1061/(ASCE)0733-9445(2007)133:11(1560).

Sarti, F., A. Palermo, and S. Pampanin. 2016a. "Development and testing of an alternative dissipative post-tensioned rocking timber wall with boundary columns." *J. Struct. Eng.* 142 (4): E4015011. https://doi.org/10.1061/(ASCE)ST.1943-541X.0001390.

Sarti, F., A. Palermo, and S. Pampanin. 2016b. "Fuse-type external replaceable dissipaters: Experimental program and numerical modeling." *J. Struct. Eng.* 142 (12): 04016134. https://doi.org/10.1061/(ASCE)ST.1943-541X.0001606.

Sarti, F., A. Palermo, and S. Pampanin. 2016c. "Quasi-static cyclic testing of two-thirds scale unbonded posttensioned rocking dissipative timber walls." *J. Struct. Eng.* 142 (4): E4015005. https://doi.org/10.1061/(ASCE)ST.1943-541X.0001291.

Sarti, F., A. Palermo, S. Pampanin, and J. Berman. 2017. "Determination of the seismic performance factors for post-tensioned rocking timber wall systems." *Earthquake Eng. Struct. Dyn.* 46 (2): 181–200. https://doi.org/10.1002/eqe.2784.

Smith, B. J., Y. C. Kurama, and M. J. McGinnis. 2011. "Design and measured behavior of a hybrid precast concrete wall specimen for seismic regions." *J. Struct. Eng.* 137 (10): 1052–1062. https://doi.org/10.1061/(ASCE)ST.1943-541X.0000327.

Sritharan, S., S. Aaleti, R. S. Henry, K.-Y. Liu, and K.-C. Tsai. 2015. "Precast concrete wall with end columns (PreWEC) for earthquake resistant design." *Earthquake Eng. Struct. Dyn.* 44 (12): 2075–2092. https://doi.org/10.1002/eqe.2576.

Structurlam. 2016. *Crosslam CLT technical design guide*. Penticton, Canada: Structurlam.

Twigden, K. M., S. Sritharan, and R. S. Henry. 2017. "Cyclic testing of unbonded post-tensioned concrete wall systems with and without supplemental damping." *Eng. Struct.* 140 (Jun): 406–420. https://doi.org/10.1016/j.engstruct.2017.02.008.

Wiebe, L., and C. Christopoulos. 2010. "Characterizing acceleration spikes due to stiffness changes in nonlinear systems." *Earthquake Eng. Struct. Dyn.* 39 (14): 1653–1670. https://doi.org/10.1002/eqe.1009.

Wiebe, L., C. Christopoulos, R. Tremblay, and M. Leclerc. 2013a. "Mechanisms to limit higher mode effects in a controlled rocking steel frame. 1: Concept, modelling, and low-amplitude shake-table testing." *Earthquake Eng. Struct. Dyn.* 42 (7): 1053–1068. https://doi.org/10.1002/eqe.2259.

Wiebe, L., C. Christopoulous, R. Tremblay, and M. Leclerc. 2013b. "Mechanisms to limit higher mode effects in a controlled rocking steel frame. 2: Large-amplitude shake table testing." *Earthquake Eng. Struct. Dyn.* 42 (7): 1069–1086. https://doi.org/10.1002/eqe.2258.

Wilson, A. 2018. "Numerical modeling and seismic performance of post-tensioned cross-laminated timber rocking wall systems." M.S. thesis, Washington State Univ.

Wilson, A. W., C. J. Motter, A. R. Phillips, and J. D. Dolan. 2019. "Modeling techniques for post-tensioned cross-laminated timber rocking walls." *Eng. Struct.* 195: 299–308. https://doi.org/10.1016/j.engstruct.2019.06.011.

Queries

1. Please provide the ASCE Membership Grades for the authors who are members.

2. Please provide street address in 1st affiliation for the author “Alex W. Wilson” in affiliation footnotes.

3. In the text “design earthquake and maximum considered earthquake for Seattle, with Site Class D”Please clarify use of “Site Class D”–there are four instances used in the article; the first two have no clarification, then the third reference refers to “location” and the fourth refers to “soil conditions.”

4. Please check the hierarchy of section heading levels.

5. ASCE Open Access: Authors may choose to publish their papers through ASCE Open Access, making the paper freely available to all readers via the ASCE Library website. ASCE Open Access papers will be published under the Creative Commons-Attribution Only (CC-BY) License. The fee for this service is $2000, and must be paid prior to publication. If you indicate Yes, you will receive a follow-up message with payment instructions. If you indicate No, your paper will be published in the typical subscribed-access section of the Journal.

6. In the text “Many of these concepts for PT precast concrete rocking walls were extended to PT LVL rocking walls”Please define at first instance “LVL” Do you mean “laminated veneer lumber (LVL)”

7. Please provide version number for "OpenSees" software.

8. Regarding “glulams”:does the edit in the text retain the intended meaning: “solely by an independent glued-laminated timber (GLT or glulams) framing system.”Please see text in following paragraph: “provided in Table 2, were determined using E-1.8E class glulams and following the design procedures”

9. Please check all figures, figure citations, and figure captions to ensure they match and are in the correct order.

10. Please check and confirm that whether we can change the variables italics in the table header for Table 5.

11. As per ASCE style only SI units are allowed, so please change "mph" into a appropriate unit (like "km/h").

12. ASCE style for math is to set all mathematical variables in italic font. Please check all math variables throughout the paper, both in equations and throughout the text, to ensure all conform to ASCE style.

13. Please provide column heading for Table 7.

14. The citation (Wiebe and Christopoulos 2009) mentioned in this sentence is not present in the References list. Please provide the full details and we will insert it in the References list and link it to this citation.

15. Please provide column heading for Table 8.

16. Does the edit in the text retain the intended meaning: “rocking walls coupled with U-shaped Flexural Plate (UFP) hysteretic damping devices”

17. Please check and confirm if updated year of publication for Akbas et al. (2017).

18. As per style, the first-author name should be followed by "et al." only if the reference has more than ten authors. Please provide all the author names instead of "et al." for reference (Akbas 2017).

19. Please provide the publisher or sponsor name and location (not the conference location) for Baird et al. (2014).

20. This query was generated by an automatic reference checking system. This reference could not be located in the databases used by the system. While the reference may be correct, we ask that you check it so we can provide as many links to the referenced articles as possible.

21. Please provide department name for Ganey (2015).

22. Please check URL–server errorsee: https://www.pci.org/PCI/Publications/PCI_Journal/Issues/1999/May-June/Seismic_Behavior_and_Design_of_Unbonded_Post-Tensioned_Precast_Concrete_Walls.aspx?WebsiteKey=5a7b2064-98c2-4c8e-9b4b-18c80973da1e)

23. This query was generated by an automatic reference checking system. This reference could not be located in the databases used by the system. While the reference may be correct, we ask that you check it so we can provide as many links to the referenced articles as possible.

24. Please check URL–server errorsee:https://www.pci.org/PCI_Docs/Design_Resources/Guides_and_manuals/references/PRESSS/Hybrid%20Post-Tensioned%20Precast%20Concrete%20Walls%20for%20Use%20in%20Seismic%20Regions.pdf

25. Please check URL: server errorSee:https://www.researchgate.net/publication/280765031_Overview_of_the_PRESSS_five-story_precast_test_building

26. Please provide the publisher or sponsor name and location (not the conference location) for Pei et al. (2018).

27. This query was generated by an automatic reference checking system. This reference could not be located in the databases used by the system. While the reference may be correct, we ask that you check it so we can provide as many links to the referenced articles as possible.

28. Please check URL: server errorSee:https://www.pci.org/PCI_Docs/Publications/PCI%20Journal/1999/Nov-Dec/Preliminary%20Results%20and%20Conclusions%20From%20the%20PRESSS%20Five-Story%20Precast%20Concrete%20Test%20Building.pdf

29. Please provide department name for Wilson (2018).

30. This reference Wilson (2018) is not mentioned anywhere in the text. ASCE style requires that entries in the References list must be cited at least once within the paper. Please indicate a place in the text, tables, or figures where we may insert a citation or indicate if the entry should be deleted from the References list.

31. Pleas e provide issue number for Wilson et al. (2018).